Annals of Nuclear Energy 149 (2020) 107775

Contents lists available at ScienceDirect

Annals of Nuclear Energy

journal homepage: www.elsevier.com/locate/anucene

On the nuclear safety improvement by post-inerting small modular reactor with stainless steel cladding

Alan Matias Avelar [a,*], Marcelo Breda Mourão [a], Marcos Maturana [b], Claudia Giovedi [b], Alfredo Yuuitiro Abe [c], Rafaela Pedrassani [d], Jian Su [d]

[a] Department of Metalurgical and Materials Engineering, Polytechnic School, University of São Paulo, Professor Mello Moraes – Cidade Universitária, 2463 São Paulo, SP Brazil
[b] Analysis, Evaluation and Risk Management Laboratory, Department of Naval Architecture and Ocean Engineering, Polytechnic School, University of São Paulo, Professor Mello Moraes – Cidade Universitária, 2231 São Paulo, SP, Brazil
[c] Nuclear and Energy Research Institute, University of São Paulo, Professor Lineu Prestes – Cidade Universitária, 2242 São Paulo, SP, Brazil
[d] Nuclear Engineering Program, COPPE, Universidade Federal do Rio de Janeiro, CP 68509 – Cidade Universitária, Rio de Janeiro, Brazil

ARTICLE INFO

Article history:
Received 6 February 2020
Received in revised form 23 July 2020
Accepted 10 August 2020
Available online 2 September 2020

Keywords:
Stainless steel
Hydrogen
Post-inerting
Small modular reactor
Containment

ABSTRACT

After Fukushima Daiichi accident, the replacement of zirconium-based fuel cladding in Light Water Reactors (LWR) became one of the main challenges of the nuclear industry. Austenitic steel–clad presents some safety advantages comparing to zirconium alloys, noticeably, higher activation energy and lower enthalpy of metal-water reaction. Thus, it produces a slower hydrogen release into the containment following a postulated accident. In this study, a Loss-of-Coolant Accident (LOCA) aggravated by the complete failure of the Emergency Core Cooling System (ECCS) is analyzed for a Small Modular Reactor (SMR). Post-accident injection of inert gas into the containment is used as one of the hydrogen control systems, to enhance safety margins during Severe Accidents (SA). The inertization system is successful in complementing Passive Autocatalytic Recombiners (PAR) to perform combustible gas control.

1. Introduction

The Fukushima Daiichi Nuclear Plant accident in March 2011 brought great challenge on the development of Accident Tolerant Fuel (ATF), which is supposed to reduce risks under beyond-design-basis accident scenarios (Terrani, 2018; Terrani et al., 2014; Pint et al., 2013; IAEA, 2009). It also reintroduced some ideas that have been studied or even practiced throughout 70 years of history of Nuclear Power Plants (NPP), including stainless steel cladding and post-inerting, as combustible gas control techniques (Abe et al., 2014; Pino et al., 2015; Massey et al., 2016; Lyu et al., 2019; Lyu et al., 2017; Peng et al., 2016; Lyu et al., 2020).

Although austenitic steel-clad fuels cannot be considered an ATF, they operated reliably in first Pressurized Water Reactors (PWRs) (Terrani et al., 2014). However, their neutron cross section is a factor of 12–16 times higher than that for Zircaloy. The enrichment penalty due to the use of stainless steel cladding became the main reason for their replacement by Zircaloy cladding (Terrani et al., 2014; Massey et al., 2016).

Zirconium fuel cladding currently used in all LWRs provides adequate material performance while being relatively transparent to neutrons produced in a reactor core. However, high-temperature interaction of Zr with water producing a large quantity of heat accompanied by hydrogen release is one of the main contributors to serious loss of integrity scenarios in nuclear reactor accidents, such as what occurred at the Three Mile Island-II and more recently at the Fukushima Daiichi-I power plants (Cathcart et al., 1977; Baker and Just, 1962; Knief, 1992). Despite being favored over stainless steel from the standpoint of neutron economy, zirconium-water reaction generates substantially more energy (1560 kcal/kg) than stainless steel (144 to 253 kcal/kg) (Knief, 1992). Due to its higher oxidation resistance up to 1100 °C, in design-basis accidents (DBA) (IAEA, 2009) stainless steel cladding may present safety advantages (Brassfield et al., 1968; Ishida et al., 1986).

However, during Severe Accidents (SA), core cooling might be interrupted, then the decay heat in the fuel and metal-water reaction enthalpy in the fuel-cladding drive the core temperature upward. As the water level decreases and core becomes uncovered, the heat transfer processes become less efficient and the fuel starts to experience physical, chemical degradation or even melting. Physical degradation occurs first ($700\,^{\circ}C - 1000\,^{\circ}C$) and involves ballooning and burst of the thin-walled cladding tube. Chemical degradation occurs at higher temperatures ($1000\,^{\circ}C - 1200\,^{\circ}C$), depending on the cladding material and is dominated by water

* Corresponding author.
E-mail address: alanmatiasavelar@gmail.com (A.M. Avelar).

https://doi.org/10.1016/j.anucene.2020.107775
0306-4549/

oxidation, which releases hydrogen and is highly exothermic (Terrani et al., 2014; Massey et al., 2016). In this case, a significant quantity of hydrogen may be released to the containment in a short period of time (Lyu et al., 2019; Lyu et al., 2017; EPRI, 2012). Although passive autocatalytic recombiners are employed in most of NPPs, these systems might not deal with full core degradation scenario. Inert gases can be employed to enhance hydrogen dilution and mixing, helping reduce hydrogen combustion risk in the containment, by keeping its volume fraction less than the flammability limit giving by Shapiro diagram (Shapiro and Moffette, 1957) whereas there is availability of oxygen (Peng et al., 2016).

Severe accident computer codes have been extensively tested in recent years (NEA, 2018; NEA, 2015; Nowack et al., 2018). These codes offer capability of modeling highly complex phenomena and various accident progressions so as to evaluate Severe Accident Management (SAM) actions, and improve its effectiveness. The principal internationally used codes today are MAAP (developed by Fauske & Associates Inc., USA), MELCOR (developed by Sandia National Laboratories, USA, under USNRC sponsorship), and ASTEC (jointly developed by IRSN, France, and the GRS, Germany) (NEA, 2018; NEA, 2015). These codes are not designed to perform best-estimate simulations, but to allow the user to bound important processes or phenomena, often using user-defined parameters. They are generally used to support Probabilistic Safety Assessment level 2 (PSA2) analyses, for a good estimate of risks for SA scenarios. Analytical methods and expert opinion on the understanding of plant systems are equally viewed as important to SAM guidelines (NEA, 2018).

In this study, a SMR scenario of Loss-of-Coolant Accident (LOCA) aggravated by complete failure of the Emergency Core Cooling System (ECCS) is analyzed. Post-accident injection of inert gas in the containment is employed to enhance combustible gas control system. Stainless steel and Zircaloy-4 performances as cladding materials are compared.

2. Materials and methods

Oxidation experiments were carried out firstly to determine metal-water reaction kinetics for Zircaloy-4 and Austenitic Stainless Steel. The kinetics equations obtained from the experiments were then applied in a simplified core model to calculate hydrogen source term evolution inside the containment. Finally, the hydrogen generation data were applied in a SMR containment model developed specifically to analyze the performance of combustible gas control systems regarding the established on 10CFR 50.44 (NRC, 2017).

2.1. Oxidation kinetics

Zircaloy-4 and Austenitic Stainless Steel samples were submitted to high temperature oxidation tests with steam. Isothermal thermo gravimetric tests at 1000, 1100, 1200, 1300 and 1350 °C were conducted inside of an electric furnace. That is the temperature range where chemical degradation significantly occurs for zirconium based cladding (Terrani et al., 2014). Chemical compositions in weight % are presented in Table 1.

Oxidation of steel by high temperature steam is highly complex, and several different oxide types are possible. Magnetite is the major product. However, other forms involving Fe, Cr, and Ni are possible. The oxidation reactions of stainless steel are as follows:

$$2Cr + Fe + 4H_2O \rightarrow FeO.Cr_2O_3 + 4H_2, \quad (1a)$$

$$3Fe + 4H_2O \rightarrow Fe_3O_4 + 4H_2, \quad (1b)$$

whereas the chemical formula for the reaction of zirconium with steam is as follows:

Table 1
Alloys compositions in mass%, determined by Inductively Coupled Plasma Atomic Emission Spectroscopy and combustion analyses.

Chemical Element	AISI 348	Zr-4
Fe	68.63	0.20
Cr	17.45	0.10
Ni	10.94	–
C	0.052	0.01
Si	0.42	–
Mn	1.61	–
P	0.017	–
Cu	–	–
V	–	–
Ta	<0.005	–
Co	0.023	–
Nb	0.83	–
S	0.003	–
B	0.0007	–
N	0.018	–
O	–	0.13
Sn	–	1.36
Zr	–	98.20

$$Zr + 2H_2O \rightarrow ZrO_2 + 2H_2. \quad (2)$$

Both oxidation behaviors may be represented by a parabolic kinetics as the oxide layer growth is controlled by diffusion through the oxide layer. The parabolic model is given by:

$$\left(\frac{\Delta m}{A}\right)^2 = A_0 \exp\left(\frac{-E_a}{RT}\right)t, \quad (3)$$

where m/A is the mass-gain per unit area $[kg.m^{-2}]$, t is time [s], A_0 is pre-exponential factor $[kg^2.m^{-4}.s^{-1}]$, E_a is the activation energy of the oxidation reaction $[J.mol^{-1}]$, R is the gas constant [8.314 $J.mol^{-1}.K^{-1}$], and T is temperature [K]. Regarding their difference in terms of thermal properties and kinetics parameters, each material will give a different profile on cladding temperature evolution.

The mass gain data were used to derive hydrogen generation rate for these materials, by using stoichiometric relations, as follows:

$$\frac{m_{H_2}}{A} = 0.1260\frac{\Delta m}{A}(T,t), \quad (4)$$

where 0.1260 is the proportional mass of hydrogen produced for each mass of oxygen reacted and m_{H_2}/A is mass of hydrogen produced per unit area $[kg.m^{-2}]$.

2.2. Simplified core model

Let us consider the core of a small modular reactor consisting of a number N_{rod} of fuel rods. Hydrogen is generated during a severe accident as a consequence of a double ended guillotine break LOCA located in cold leg aggravated by complete failure of the ECCS. The temperature evolution in the SMR core is determined by a simplified core model. For a conservative simulation, an adiabatic boundary is imposed on the surface of the fuel rods by neglecting the heat transfer between the fuel rods and the vapor in the reactor core. The volumetric heat generation rate $q_f^{(i)}(z,t)$ at i-th fuel rod is specified by a given axial profile and the decay heat power as a function of time following ANSI/ANS 5.1-2014 (ANS, 2014). The kinetics parameters are used to determine hydrogen generation rate and energy release by metal-water reaction. The outer radius of the fuel pellet, inner and outer radius the cladding are R_{fo}, R_{ci} and R_{co} respectively. The active height of the reactor core is L. The temperature distributions in the fuel and cladding of all fuel rods in the reactor core are determined by solving the transient heat conduc-

tion equations in fuel and cladding of each fuel rod, for a total of N_{rod} fuel rods, written as follows:

$$\rho_f Cp_f \frac{\partial T_f^{(i)}(r,z,t)}{\partial t} = \frac{1}{r}\frac{\partial}{\partial}\left(r\, k_f(T)\frac{\partial T_f^{(i)}(r,z,t)}{\partial r}\right) + q_f^{(i)}(z,t), \quad 0 < r < R_{fo}, \quad -L/2 < z < L/2, \quad i = 1,\ldots,N_{rod}, \tag{5a}$$

$$\rho_c Cp_c \frac{\partial T_c^{(i)}(r,z,t)}{\partial t} = \frac{1}{r}\frac{\partial}{\partial}\left(r\, k_c(T)\frac{\partial T_c^{(i)}(r,z,t)}{\partial r}\right) + q_c^{(i)}(z,t), \quad R_{ci} < r < R_{co}, \quad -L/2 < z < L/2, \quad i = 1,\ldots,N_{rod}, \tag{5b}$$

where $T_f^{(i)}$ and $T_c^{(i)}$ are temperatures in fuel and cladding of i-th fuel rod, ρ_f and ρ_c their densities, Cp_f and Cp_c the specific heats, k_f and k_c the thermal conductivities. $q'''_{i,f}$ and $q'''_{i,c}$ the volumetric heat generation rates in fuel and cladding of i-th fuel rod. h_g is the heat transfer coefficient for the gap, and h the heat transfer coefficient between the cladding and the coolant.

Eqs. (5) are to be solved with the following boundary and interface conditions:

$$\left.\frac{\partial T(i)_f(r,z,t)}{\partial r}\right|_{r=0}, \quad \text{at} \quad r = 0, \tag{6a}$$

$$-R_{fo}k_f \left.\frac{\partial T_f^{(i)}(r,z,t)}{\partial r}\right|_{r=R_{fo}} = R_g h_g (T_f^{(i)}(R_{fo},z,t) - T_c^{(i)}(R_{ci},z,t)), \tag{6b}$$

$$-R_{ci}k_c \left.\frac{\partial T_c^{(i)}(r,z,t)}{\partial r}\right|_{r=r_{ci}} = R_g h_g (T_f^{(i)}(R_{fo},z,t) - T_c^{(i)}(R_{ci},z,t)), \tag{6c}$$

$$-k_c \left.\frac{\partial T_c^{(i)}(r,z,t)}{\partial r}\right|_{r=R_{co}} = h(T_c^{(i)}(R_{co},t) - T_m^{(i)}(z,t)), \tag{6d}$$

and the initial conditions specified at the beginning of the simulation

$$T_f^{(i)}(r,z,0) = T_{f0}^{(i)}(r,z), \tag{7a}$$

$$T_c^{(i)}(r,0) = T_{c0}^{(i)}(r). \tag{7b}$$

We consider that the convective heat transfer between the cladding surface and the coolant is negligible and the heat transfer coefficient h can be taken as zero. The convective boundary condition (6d) becomes an adiabatic boundary condition at the cladding outer radius (R_{co}) of all fuel rods.

$$-k_c \left.\frac{\partial T_c^{(i)}(r,z,t)}{\partial r}\right|_{r=R_{co}} = 0. \tag{8}$$

Eqs. (5) together with the boundary, interface and initial conditions (6) and (7) are solved by using a finite difference method.

2.3. Containment model

Afterwards, a simplified SMR containment model was developed using SCILAB and Excel Visual Basic for Applications (VBA) codes to analyze the performance of different combustible gas control systems. Fig. 1 shows the SMR containment model and also the main heat sources considered in the analysis.

The simplifications and assumptions of the SMR containment model are listed in Table 2.

The simplifications 1 to 4 are related to typical core phenomena whereas the others are related to containment phenomena. They were used to maximize the hydrogen generation in order to challenge the combustible gas control systems. The fourth assumption is considered to be appropriate only for Iron based cladding where cross-sectional area remains largely unchanged up to the point of burst, unlike zirconium based alloys (Massey et al., 2016). However, when melting point is reached, fuel rod integrity is assumed to be lost and the entire cladding mass is converted to form hydrogen.

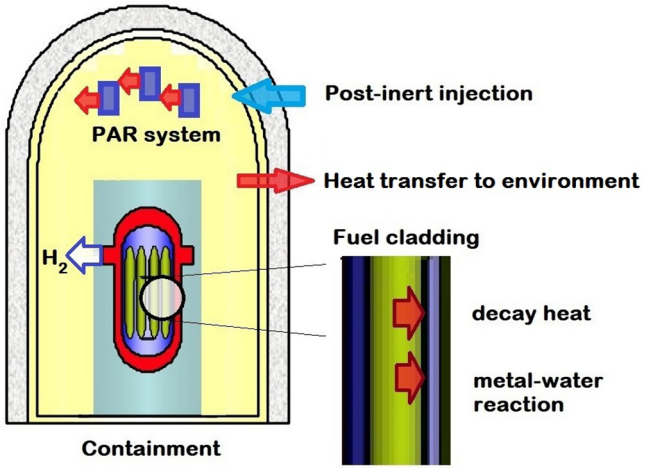

Fig. 1. Containment model considering hydrogen source term, main heat sources and combustible gas control systems.

Table 2
Simplifications and assumptions of the SMR containment model.

Simplifications and Assumptions	Phenomena/ Context
1. Adiabatic fuel rods.	Core heat transfer
2. Hydrogen is generated only by metal-water reaction.	Hydrogen source term
3. Steam is always available to react.	Metal-water reaction
4. Fuel rod geometry (oxidation area) is kept constant until the melting point.	In-Vessel core degradation
5. Constant overall heat transfer coefficient.	Containment heat transfer
6. Raoult's law is used to calculate vapor pressures of all species (vapor mixture acts as an ideal gas).	Containment thermodynamics
7. Reactor Pressure Vessel (RPV) high-point venting releases hydrogen to containment.	Containment pressure load and Ex-vessel hydrogen combustion risk
8. Uniform hydrogen distribution (single compartment).	Containment mass transfer
9. Nitrogen is used as inert gas.	Mitigation of hydrogen combustion risk

The containment has a small free volume of approximately 650 m^3. There is a corridor located at the upper part of containment that communicates all areas and the ventilation system is considered to provide uniform distribution of the gases. Thus, a single control volume was adopted. There is no accumulation of hydrogen neither in the RPV, nor in the primary system. This is assumed due to RPV venting and also to increase combustion risk and challenge combustible gas control systems. The steel containment is surrounded by water that provides a fast condensation. Thus, pressure and temperature rapidly decrease after LOCA. The SMR model was verified taking into account code intercomparison against a MELCOR SMR model (Humphries et al., 2017; Humphries et al., 2017).

The hydrogen produced is considered to be released from the core into the containment instantaneously. Such assumptions (adiabatic core as boundary condition and instantaneous release) ensure a faster clad heat up and consequently an earlier hydrogen production and release to the containment. At the end of the simulation time, the total mass of hydrogen release to the containment is equivalent to that generated by a 100% fuel-clad metal water reaction.

Let us consider a reactor containment with volume V and heat transfer area A with the environment. At an initial instant, the pressure in the containment is $P(0)$, and the temperature is $T(0)$. We

are interested in analyzing the time evaluation of the concentrations of several species in the containment, namely the nitrogen N_2, oxygen O_2, hydrogen H_2 and water H_2O. The initial masses of the components in the containment are $M_{N_2}(0), M_{O_2}(0), M_{H_2}(0), M_{H_2O}(0)$ respectively. It is assumed that thermodynamic properties as function of temperature are available for all components, for example the saturation pressure $P_{sat}(T_{sat})$, the specific internal energy $u_{N_2}(T), u_{O_2}(T), u_{H_2}(T), u_g(T), u_f(T)$, specific enthalpy $h_{N_2}(T), h_{H_2}(T)$ and specific volumes $v_g(T), v_f(T)$. Containment conditions were calculated using a simplified thermodynamic model, which consists of conservation equations for the mass of each species and for total energy in the containment:

$$\frac{dM_{N_2}}{dt} = \dot{m}_{N_2,in}, \tag{9a}$$

$$\frac{dM_{O_2}}{dt} = -\dot{m}_{O_2,rec}, \tag{9b}$$

$$\frac{dM_{H_2}}{dt} = \dot{m}_{H_2,in} - \dot{m}_{H_2,rec}, \tag{9c}$$

$$\frac{dM_{H_2O}}{dt} = \dot{m}_{H_2O,rec}, \tag{9d}$$

$$\frac{d}{dt}(U_{Total}) = \dot{m}_{N_2,in}\left(h_{N_2} + \frac{v_{N_2}^2}{2}\right) + \dot{m}_{H_2,in}\left(h_{H_2} + \frac{v_{H_2}^2}{2}\right) + \dot{Q} - U_{ht}A(T - T_e). \tag{10}$$

The total energy U_{Total} is given by

$$U_{Total} = M_{N_2}u_{N_2} + M_{O_2}u_{O_2} + M_{H_2}u_{H_2} + M_{H_2O}(x_{H_2O}u_g + (1 - x_{H_2O})u_f) \tag{11}$$

where u is the specific internal energy, h specific enthalpy, v is velocity, $\dot{m}$ is the mass flow rate, x_{H_2O} is the mass fraction of water vapor (static quality), U_{ht} is the overall heat transfer coefficient, and T_e is the environment temperature. As the specific energies and enthalpies are functions of temperature, the temperature $T(t)$ in the containment is readily obtained from the total energy, Eq. (11). The heating power $\dot{Q}$ is comprised of the reactor decay heat power, the heat generation of metal-water reaction, and the heat generation of recombination from the catalysts. An analytical solution of the containment model is obtained with linearized thermodynamic properties, and constant hydrogen generation and nitrogen injection rates. The analytical solution is given in the Appendix for a comparison with the numerical solution of the containment model.

To determine the species partial pressures in the gas phase, the containment was considered an ideal system, where ideal liquid and ideal vapor are assumed to be in equilibrium at each time step. In this case, Raoult's law is combined with Dalton's Law. The partial pressures of the species are determined as

$$\begin{aligned} P_{N_2} &= \frac{n_{N_2}R_{N_2}T}{V_c}, \quad P_{O_2} = \frac{n_{O_2}R_{O_2}T}{V_c}, \\ P_{H_2} &= \frac{n_{H_2}R_{H_2}T}{V_c}, \quad P_{H_2O} = P_{sat}(T), \end{aligned} \tag{12}$$

where R is the gas constant. The containment pressure is obtained as the sum of the partial pressures:

$$P = P_{N_2} + P_{O_2} + P_{H_2} + P_{H_2O}. \tag{13}$$

The mole fractions of the species in the gas phase are determined by the ratios between the partial pressures and the total pressure in the containment:

$$y_{N_2} = \frac{P_{N_2}}{P}, \quad y_{O_2} = \frac{P_{O_2}}{P}, \quad y_{H_2} = \frac{P_{H_2}}{P}, \quad y_{H_2O} = \frac{P_{H_2O}}{P}. \tag{14}$$

Passive Autocatalytic Recombiners (PAR) system is considered to be functional. The PAR model is described by Eqs. 15 and 16 (Arnould et al., 2001).

$$\dot{m}_{H_2,rec} = 0.4C_{H_2}P\left(\frac{293}{T}\right)^{1.5}\tanh(C_{H_2} - 0.5)A(C_{H_2}, C_{O_2}) \tag{15}$$

where $\dot{m}_{H_2,rec}$ is the hydrogen recombination rate $[kg/h], C_{H_2}$ is hydrogen concentration in vol.%, C_{O_2} is oxygen concentration in vol.% and P is total pressure $[bar]$.

$$\begin{cases} A = 1, & \text{if}, \quad C_{H_2} \leqslant C_{O_2} \\ A = 0.6, & \text{if}, \quad C_{H_2} > C_{O_2} \\ A = 0.33, & \text{if}, \quad C_{O_2} < 4\% \end{cases} \tag{16}$$

PAR system is used to provide a passive combustible gas control. However, once post-accident inerting system is activated, the overpressure increases hydrogen depletion rate by recombiners, which according to Eq. 15, is pressure dependent (Lyu et al., 2017).

Nitrogen and carbon dioxide are usually used as inert gas in post-inerting (Lyu et al., 2019). In this study, N_2 is selected as inert gas due its wide application experience in Boiling Water Reactors (BWR) plants, which are pre-inerted (Camp et al., 1983). The inerted atmosphere criterion is an atmosphere with less than 4% oxygen by volume (NRC, 2017). PAR are considered to be active in low oxygen concentrations. However, their performance in oxygen poor atmosphere is corrected by Eq. 16, where the depletion rates are lowered by a factor of 3.

Post-inerting system was modeled by a control valve with constant upstream pressure. Liquefied nitrogen is stored in a tank. For supply, the liquid is vaporized and injected at 6 bar and 10 °C to avoid jeopardizing containment integrity. The start of injection considered a sensitivity analysis on the activation time in order to discover the maximum possible delay without reaching the flammability limits. N_2 mass flow rate is calculated supposing incompressible flow. It depends on the containment backpressure, which is time dependent due to condensation and nitrogen injection, according to the following equation:

$$\dot{m}_{N_2} = \sqrt{\frac{6 - P(t)}{K}} \tag{17}$$

where $\dot{m}_{N_2}$ is nitrogen mass flow rate $[kg/s], K$ is a hydraulic parameter $[bar.s^2.kg^{-2}]$ and P is the containment back pressure [bar].

3. Results and discussion

Metal-water reaction kinetics for Zircaloy-4 and Austenitic Stainless Steel are described in SubSection 3.1. The evolution of hydrogen source term inside containment for both alloys and the performance of combustible gas control systems were analyzed using the SMR containment model. The results are described in SubSection 3.2.

3.1. Oxidation kinetics

Weight gain results for Zircaloy-4 are similar to previous studies (Cathcart et al., 1977; Baker and Just, 1962; Urbanic and Heidrick, 1978). Austenitic Stainless Steel also performed similar to previous studies (Ishida et al., 1986; Brassfield et al., 1968). Conventional austenitic stainless steel claddings with 18-Cr and 8-Ni are more oxidation resistant than Zircaloy but do not contain sufficient Cr and Ni levels to be protective at 1200 °C and higher temperatures. Furthermore, concerning the metal-water reaction as an important heat source, stainless steel is favored against Zircaloy. Focusing on the kinetic parameters, it can be seen in Fig. 2 that the austenitic stainless steel has a higher activation energy comparing to Zircaloy-4. This will lead to a considerably slower oxidation in case of austenitic stainless steel cladding that will affect significantly the hydrogen production. Kinetic parameters obtained for each material are presented in Table 3. These results

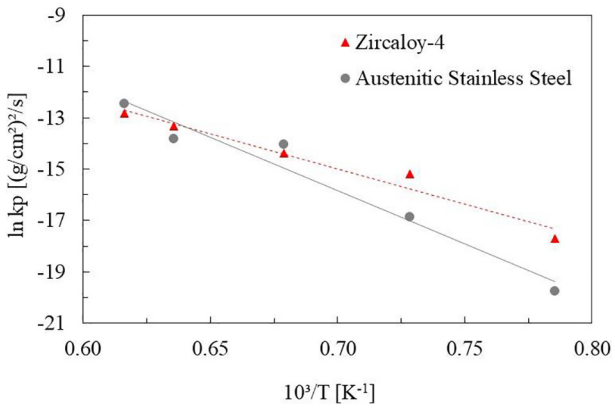

Fig. 2. Arrhenius plot of the parabolic weight-gain rate constants for materials oxidized in 100% water environment.

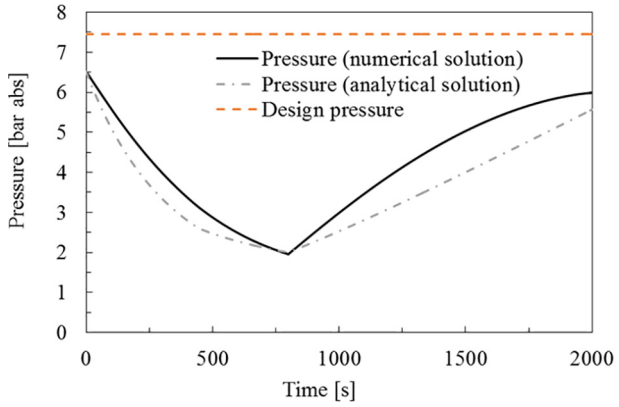

Fig. 3. Containment pressure evolution during post-LOCA scenario with ECCS failure and post-inerting system actuation on Austenitic Stainless Steel (SS) case.

Table 3
Arrhenius parameters of parabolic kinetic models of Austenitic SS and Zircaloy-4.

Arrhenius Parameters	Austenitic SS	Zr-4
A_0 ($kg^2/m^4/s$)	4.8×10^7	119
E_a (kJ/mol)	344	176

were applied in the SMR containment model to predict hydrogen generation for each material.

Oxidation of $Fe - Cr - Ni$ alloys is highly dependent on Cr content. Chromium levels greater than 20% led to the formation of a predominantly chromic oxide scale with the associated low diffusion rates through the scale and hence low oxidation rates. Pint et al. (2013) showed that 25% Cr was needed to form a protective Cr_2O_3 scale at 1200 °C (Pint et al., 2013). The oxidation resistance is an important challenge for finding other cladding materials (Terrani, 2018).

3.2. Containment analysis

The simulation of the containment transient happens according to the following time frame: Large Break Loss-of-Coolant-Accident (LBLOCA) peak pressure in the containment is the initial condition (0 s). The following 500 s reveals the importance of steam condensation to reduce containment pressure, which is necessary to allow post-inert agent injection, which according to Fig. 3 starts at 800 s.

Zircaloy cladding temperature evolution was faster than Stainless Steel. Thus, the initial hydrogen production is delayed by approximately 250 s on the Austenitic Stainless Steel case. According to Fig. 4, as hydrogen generation evolution is faster on Zircaloy case, a higher quantity of hydrogen is released at the very beginning of core oxidation and the flammability limit is reached, even though the PAR systems is considered to be functional. Whereas, on Austenitic Stainless Steel case flammability limit is not reached. The delayed hydrogen generation on Austenitic Stainless Steel case can be better seen in Fig. 5, where it is compared with Zircaloy case throughout the entire simulation time.

Considering the activation of post-inerting system, Fig. 6 shows that in both cases oxygen concentration reduction is accelerated by the injection of nitrogen (which starts at 800 s). In both cases, it quickly brings the oxygen concentration to 4% vol., when the atmosphere is considered to be inert (NRC, 2017). On the Austenitic Stainless Steel case it happens at 1200 s, whereas on Zircaloy case it happened earlier (at approximately 900 s), mainly due its higher hydrogen concentration, which helps reducing oxygen partial pressure.

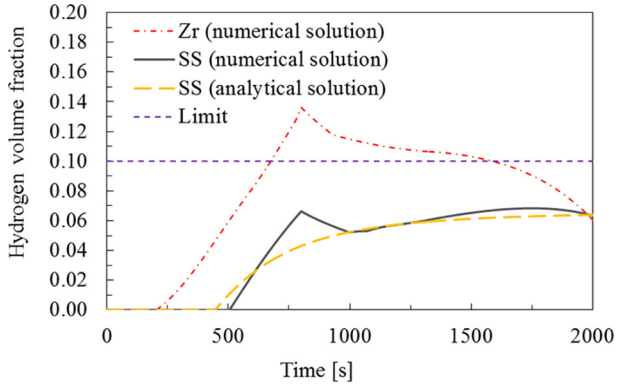

Fig. 4. Hydrogen volume fraction evolution in containment Zircaloy (Zr) case comparing to Austenitic Stainless Steel (SS) case and 10CFR 50.44 limit (19).

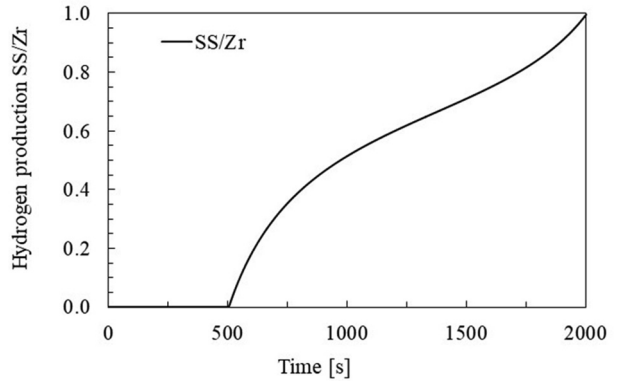

Fig. 5. Comparison between hydrogen production on Austenitic Stainless Steel (SS) case divided by Zircaloy (Zr) case.

Even though the same combustible gas control system is considered in both cases, the results for Zircaloy cladding showed a higher probability of hydrogen combustion (deflagration, Deflagration to Detonation Transition (DDT) or even detonation) once, according to Fig. 4, the flammability limit is reached (NRC, 2017). However, on the Austenitic Stainless Steel case, hydrogen concentration is kept under 7% vol.

An analytical solution is presented in the Appendix to verify the SMR containment model. Verification is concerned with identifying and removing errors in the model by comparing numerical solutions to analytical solution (Schlesinger, 1979; Thacker et al.,

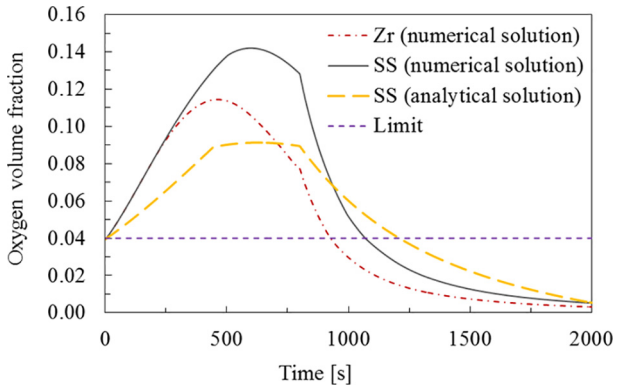

Fig. 6. Oxygen volume fraction evolution in containment Zircaloy (Zr) case comparing to Austenitic Stainless Steel (SS) case and 10CFR 50.44 inerted atmosphere limit (NRC, 2017).

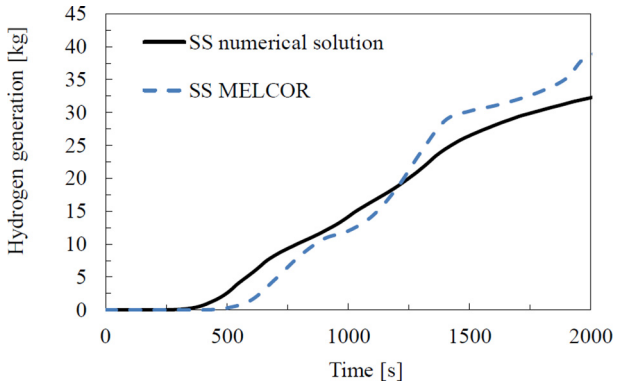

Fig. 8. Comparison of hydrogen source term evolution in containment results obtained with SMR containment model and MELCOR.

2004). The numerical solution presented significant sensitivity concerning the time step. Nevertheless, a good qualitative agreement was obtained.

Validation, on the other hand, is concerned with quantifying the accuracy of the model by comparing numerical solutions to experimental data. As very little experimental data exist for this purpose presently and they are concerned about Large Dry containments, a future work should be focused on this area, specifically to SMR containments (Tiltmann et al., 1993).

The hydrogen combustion is in general inferred from the well-known Shapiro diagram (Shapiro and Moffette, 1957) which predicts Flammability and Detonation Limits of hydrogen-air–steam mixtures. Flammability limits from the original diagram were changed in order to consider the downward propagation limits from (Camp et al., 1983) and also to be consistent with 10CFR 50.44 (NRC, 2017) criterion of 10 % vol. as maximum allowable hydrogen concentration. According to Fig. 7, Zircaloy case also showed the possibility of hydrogen combustion, which does not happen on the Austenitic Stainless Steel case.

3.3. Code-to-code comparison

SA codes are often used for hydrogen source term calculations. However, they require a careful examination of modeling assumptions. Considering the high uncertainty of simulation results, code-to-code comparison can provide a deeper understanding of simulated phenomena.

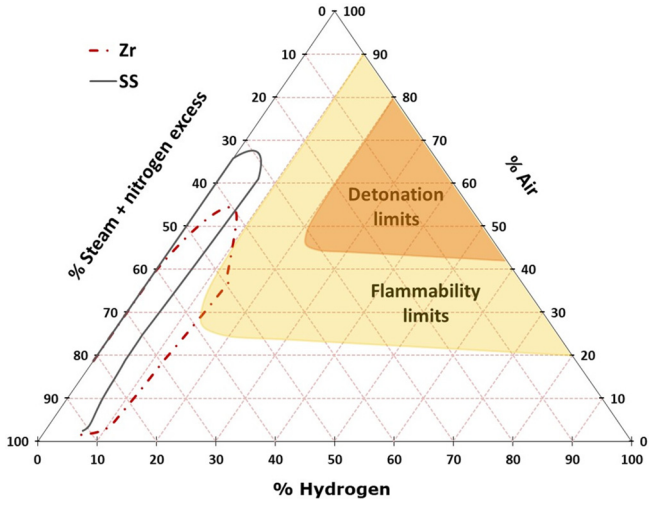

Fig. 7. Shapiro diagram highlighting the state of the containment with respect to the flammability limits during simulation performed using SMR containment model comparing Zircaloy (Zr) case and Austenitic Stainless Steel (SS) case. Flammability limits consider the downward propagation limits (Camp et al., 1983).

The same accident scenario studied with SMR model was simulated with MELCOR. First, Zircaloy was employed as cladding material in order to utilize MELCOR default settings. Then, Stainless Steel as cladding material was considered by implementing the related material properties into MELCOR. Fig. 8 shows that the hydrogen generation evolution considering Austenitic Stainless Steel (SS) is in good agreement with MELCOR prediction. Similarly, the hydrogen volume fraction evolution in containment predicted by SMR model is also in agreement with MELCOR results.

Concerning the oxidation resistance of different cladding materials, it is clear that the process shall be studied from an experimental point of view. The kinetic data provides crucial support for validation.

Fuel rod swelling and also cladding burst might lead to an increase of oxidation area whose consequence is a faster hydrogen generation evolution. The calculation accuracy could be improved by using more realistic conditions, for example, by applying thermal–hydraulics parameters for realistic accident situations (instead of an adiabatic boundary condition) and by properly taking into account cladding embrittlement during loss-of-coolant accidents.

The containment model was also validated by considering a scenario in which nitrogen injection started at 300 s. Initial conditions and input data for SMR containment were obtained using RELAP results for loss-of-coolant accident whereas MELCOR model could gather the entire simulation without any need of code coupling. Figs. 9–11 show good agreement between the results of

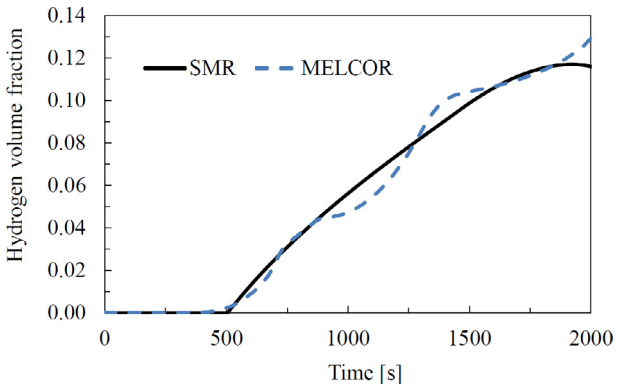

Fig. 9. Comparison of hydrogen volume fraction evolution results obtained with SMR containment model and MELCOR.

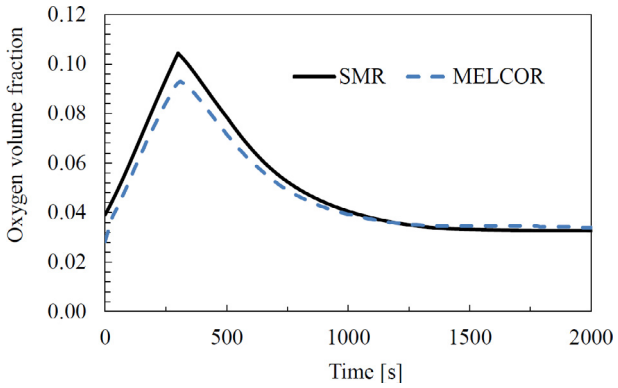

Fig. 10. Comparison of oxygen volume fraction evolution results obtained with SMR containment model and MELCOR.

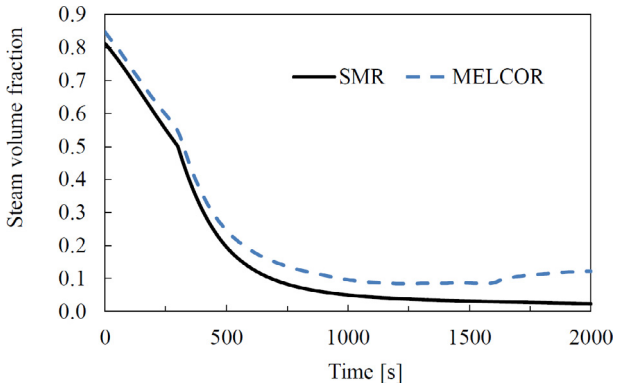

Fig. 11. Comparison of steam volume fraction evolution results obtained with SMR containment model and MELCOR.

hydrogen, oxygen and steam volume fractions predicted by the SMR model and MELCOR, respectively.

It is worth mentioning that there are other aspects not covered by the current study, for example: fission product release and transport, corium interactions and hydrogen combustion regimes in SA conditions. The present work was limited to comparing the performance of different cladding materials considering an accident scenario. The advantage of stainless steel cladding is shown by analyzing containment variables, especially hydrogen concentration.

4. Conclusions

Fukushima accident raised a question of what can be considered as 'proven technology' on beyond design basis accidents. This paper revisits some technologies in order to improve nuclear safety in SMRs, by considering Austenitic Stainless Steel as cladding material instead of Zircaloy-4, and adding a post-inerting system to assist PAR system on combustible gas control. The former would provide a slower accident progression, while the latter would be able to enhance combustible gas control performance in a more severe scenario. The main conclusions of the work are as follows:

(1) Stainless steel cladding shows an improvement of safety by reducing heat sources due to its less exothermic metal-water reaction compared to zirconium alloys.
(2) Post-inerting systems assists combustible gas control by: enhancing the mixing process and reducing hydrogen partial pressure, and also overcomes eventual difficulties like PAR allocation and lack of oxygen available for recombination.
(3) SMR containment makes post-inertization system feasible due to its limited free volume, which results in shorter period of time to achieve an inert atmosphere.
(4) The proposed technologies would improve safety margins on avoiding the possibility of hydrogen combustion inside containment. However, more studies are needed to demonstrate that post-accident atmosphere will not support hydrogen combustion and that inadvertent actuation can be safely accommodated during plant operation.
(5) Despite the gain of hydrogen dilution due to post-inerting, the SMR must ensure that containment filtration and discharge system is functioning properly at accident conditions to prevent containment from overpressure. Also, radiological consequences resulting from the purge of the containment shall be analyzed.

Declaration of Competing Interest

The authors declare that they have no known competing financial interests or personal relationships that could have appeared to influence the work reported in this paper.

Acknowledgments

The authors are grateful for the support from CAPES, FAPERJ, and CNPq and for Gil Teixeira Sobrinho and Fernando Lage Araújo Schweizer on technical discussions.

Appendix A. Analytical model for containment pressurization

To obtain an analytical solution, linearised thermodynamic properties are generated from the accurate thermodynamic data, as follows:

$$u^*_{N_2}(T) = a_{N_2}T + b_{N_2}, \tag{16a}$$

$$h^*_{N_2}(T) = c_{N_2}T + d_{N_2}, \tag{16b}$$

$$u^*_{H_2}(T) = a_{H_2}T + b_{H_2}, \tag{16c}$$

$$h^*_{H_2}(T) = c_{N_2}T + d_{H_2}, \tag{16d}$$

$$u^*_{O_2}(T) = a_{O_2}T + b_{O_2}, \tag{16e}$$

$$v^*_f(T) = e_{H_2O}T + f_{H_2O} \tag{16f}$$

$$\left(\frac{u_g(T)}{v_g(T)}\right)^* = a_{H_2O}T + b_{H_2O}, \tag{16g}$$

$$\left(\frac{u_f(T)}{v_g(T)}\right)^* = c_{H_2O}T + d_{H_2O}. \tag{16h}$$

It is assumed that the gas generation or injection rates is constant within a given time internal. Typically, we divide the simulation process in three stages. At stage I ($0 \leqslant t \leqslant t_1$), there is no hydrogen generation or nitrogen injection; at stage II ($t_1 \leqslant t \leqslant t_2$), there is only hydrogen generation but no nitrogen injection; the hydrogen generation rates at stage II is given by:

$$\dot{m}^{(II)}_{H_2} = \beta^{(II)}_{H_2}. \tag{17}$$

At stage III ($t_2 \leqslant t \leqslant t_3$), there are both hydrogen generation and nitrogen injection,

$$\dot{m}^{(III)}_{H_2} = \beta^{(III)}_{H_2}, \quad \dot{m}^{(III)}_{N_2} = beta^{(III)}_{N_2}. \tag{18a, b}$$

The mass conservation equations for the four components are given by Eqs. (9). The energy conservation equation for the containment is described by Eq. (10). The total energy conservation in the containment is given by:

$$U^i(t) = M^i_{N_2} u_{N_2}(T) + M^i_{O_2} u_{O_2} + M^i_{H_2} u_{H_2}(T) + \frac{V}{v_{g_f}} u_g(T) + (M_{H_2O} - \frac{V}{v_{g_f}}) u_f(T). \quad (19)$$

The mass conservation Eqs. (9) are integrated in time to obtain the masses of the components as a function of time.

$$M^i_{N_2}(t) = \beta^i_{N_2} t + \gamma^i_{N_2}, \quad (20a)$$

$$M^i_{O_2} = M_{O_2}(0) = M_{O_2}, \quad (20b)$$

$$M^i_{H_2}(t) = \beta^i_{H_2} t + \gamma^i_{H_2} \quad (20c)$$

$$M^i_{H_2O} = M_{H_2O}(0) = M_{H_2O}. \quad (20d)$$

The solutions given in Eqs. (20) and the linearized thermodynamic proprieties are used in the energy conservation Eq. (10), which becomes:

$$(A_1 + A_2 t_0)\left(\frac{\mathrm{d}\, T(t)}{\mathrm{d}\, t}\right) = B_1 + B_2 T(t), \quad (21)$$

to be solved with the initial condition:

$$T(0) = T_0. \quad (22)$$

The analytical solution of Eq. (21) is given by:

$$T(t) = -\frac{B_1}{B_2} + (A_1 + A_2 t)^{\frac{B_2}{A_2}} C_1, \quad (23)$$

where C_1 is a constant to be determined by the initial condition on Eq. (22)

$$C_1 = A_1^{-\frac{B_2}{A_2}}\left(T_0 + \frac{B_1}{B_2}\right). \quad (24)$$

The analytical solution for the containment temperature $T(t)$ is thus given by:

$$T(t) = -\frac{B_1}{B_2} + A_1^{\frac{-B_2}{A_1}}\left(T_0 + \frac{B_1}{B_2}(A_1 + A_2 t)\right)^{\frac{B_2}{A_2}}, \quad (25)$$

where:

$$A_1 = a_{N_2} M_{N_2 0} + a_{O_2} M_{N_2 O} + a_{O_2} M_{O_2}, \quad (26a)$$

$$A_2 = a_{N_2} b_{N_2} + a_{O_2} b_{N_2}, \quad (26b)$$

$$B_1 = -b^2_{N_2} + b_{H_2} d_{H_2} + b_{N_2}(d_{H_2} - b_{O_2}) + Q - U_{h_t} A T_e, \quad (26c)$$

$$B_2 = -a_{N_2} b_{N_2} - a_{O_2} b_{N_2} + b_{H_2} C_{H_2} + b_{N_2} C_{N_2} + U_{h_t} A. \quad (26d)$$

Once the containment temperature $T(t)$ is obtained, the containment pressure $P(t)$ and the mole fractions of the species can be readily obtained.

References

Abe, A., Giovedi, C., Gomes, D.D.S., Teixeira e Silva, A., 2014. Revisiting stainless steel as PWR fuel rod cladding after Fukushima Daiichi Accident. J. Power Energy Eng. 8, 973–980.

Arnould, F., Bachellerie, E., Auglaire, M., de Boeck, B., Braillard, O., Eckardt, B., Ferroni, F., Moffett, R., Van Goethem, G., 2001. State of art on hydrogen passive autocatalytic recombiner. Report FR0200284, European Union PARSOAR Project..

ANS, 2014. Decay heat power in light water reactors. Report ANSI/ANS-5.1-2014, La Grange Park: American Nuclear Society, Standards Committee..

Baker Jr, L., Just, L.C., 1962. Studies of metal-water reactions at high temperatures experimental and theoretical studies of the zirconium-water reaction. Report ANL-6548, Argonne National Lab. (ANL), Argonne, IL (United States)..

Brassfield, H., White, J., Sjodahl, L., Bittel, J., 1968. Recommended property and reaction kinetics data for use in evaluating a light-water-cooled reactor loss of coolant incident involving Zircaloy-4 or 304SS clad UO2. Report GEMP-482, General Electric Co., Cincinnati, OH (United States). Missile and Space Division.

Camp, A.L., Cummings, J.C., Sherman, M.P., 1983. Light water reactor hydrogen manual. NUREG/CR-2726. Report SAND 82-1137, Sandia National Laboratories..

Cathcart, J., Pawel, R., McKee, R., Druschel, R., Yurek, G., Campbell, J., Jury, S., 1977. Zirconium metal-water oxidation kinetics, iv: Reaction rate studies. Report ORNL/NUREG-17, Oak Ridge National Lab..

EPRI, 2012. Severe accident management guidance technical basis report - volume 2: The physics of accident progression. Report 1025295, Institute, Electric Power Research..

Humphries, L., Beeny, B., Gelbard, F., Louie, D., Phillips, J., 2017a. MELCOR computer code manuals, vol. 1: Primer and users' guide, version 2.2.9541. Report SAND 2017-0455 O, Sandia National Laboratories..

Humphries, L., Beeny, B., Gelbard, F., Louie, D., Phillips, J., 2017b. MELCOR computer code manuals, vol. 2: Reference manual, version 2.2.9541. Report SAND 2017-0876 O, Sandia National Laboratories..

IAEA, 2009. Deterministic Safety Analysis for Nuclear Power Plants. IAEA Specific Safety Guide.

Ishida, T., Harayama, Y., Yaguchi, S., 1986. Oxidation of 304 stainless steel in high-temperature steam. J. Nucl. Mater. 140, 74–84.

Knief, R.A., 1992. Nuclear Engineering. Theory and Technology of Commercial Nuclear Power. Hemisphere Publishing Corporation, Washington.

Lyu, X., Lee, X., Ji, K., Yu, Y., Wang, S., 2017. Impact of inert gas injection rate on reducing hydrogen risk during AP1000 post-inerting. Annals Nucl. Energy 110, 230–233.

Lyu, X., Meng, X., Wang, B., Niu, F., Liu, S., Huang, X., Yin, H., 2019. Analysis of different inert gas injection point's influence on hydrogen risk during post-inerting in nuclear power plant. Annals Nucl. Energy 129, 249–252.

Lyu, X., Wang, B., Liu, S., Huang, X., Meng, X., 2020. Effect on hydrogen risk of total amount of inert gas during post-inerting in AP1000 npp. Annals Nucl. Energy 140, 107125.

Massey, C.P., Terrani, K.A., Dryepondt, S.N., Pint, B.A., 2016. Cladding burst behavior of Fe-based alloys under LOCA. J. Nucl. Mater. 470, 128–138.

Nowack, H., Chatelard, P., Chailan, L., Hermsmeyer, S., Sanchez, V., Herranz, L., 2018. CESAM – code for european severe accident management, EURATOM project on ASTEC improvement. Annals Nucl. Energy 116, 128–136.

NEA, 2015. Status report on hydrogen management and related computer codes. Report NEA/CSNI/R(2014) 8, Committee on the Safery of Nuclear Installations, Nuclear Energy Agency, OECD..

NEA, 2018. Informing severe accident management guidance and actions for nuclear power plants through analytical simulation. Report NEA/CSNI/R(2017) 16, Committee on the Safery of Nuclear Installations, Nuclear Energy Agency, OECD..

NRC, 2017. 10CFR Part 50.44 combustible gas control for nuclear power reactors. Journal article, Nuclear Regulatory Commission U.S.

Peng, C., Tong, L., Cao, X., 2016. Numerical analysis on hydrogen stratification and post-inerting of hydrogen risk. Annals Nucl. Energy 94, 451–460.

Pino, E.S., Abe, A.Y., Giovedi, C., 2015. The quest for safe and reliable fuel cladding materials. In: Proceedings of 2015 International Nuclear Atlantic Conference (INAC 2015), São Paulo, Brazil. ABEN.

Pint, B.A., Terrani, K.A., Brady, M.P., Cheng, T., Keiser, J.R., 2013. High temperature oxidation of fuel cladding candidate materials in steam-hydrogen environments. J. Nucl. Mater. 440, 420–427.

Schlesinger, S., 1979. Terminology for model credibility. Simulation 32 (3), 103–104.

Shapiro, Z., Moffette, T., 1957. Hydrogen flammability data and application to PWR loss-of-coolant accident. Report WAPD-SC-545, Westinghouse Electric Corp., Pittsburgh, PA (United States). Bettis Plant.

Terrani, K.A., 2018. Accident tolerant fuel cladding development: promise, status, and challenges. J. Nucl. Mater. 501, 13–30.

Terrani, K.A., Zinkle, S.J., Snead, L.L., 2014. Advanced oxidation-resistant iron-based alloys for LWR fuel cladding. J. Nucl. Mater. 448, 420–435.

Thacker, B.H., Doebling, S.W., Hemez, F.M., Anderson, M.C., Pepin, J.E., Rodriguez, E. A., 2004. Concepts of model verification and validation. Report..

Tiltmann, M., Risse, D., Pana, P., Huettermann, B., Rohde, J., 1993. Post-inerting of a large dry containment in beyond-design-basis accidents in PWR plants. a survey of existing studies with an initial assessment. Tech. rep., Gesellschaft fuer Anlagen-und Reaktorsicherheit (GRS) mbH..

Urbanic, V., Heidrick, T., 1978. High-temperature oxidation of Zircaloy-2 and Zircaloy-4 in steam. J. Nucl. Mater. 75 (2), 251–261.